Understanding the optical properties of $ZnO_{1-x}S_x$ and $ZnO_{1-x}Se_x$ alloys

Gustavo Baldissera and , and Clas Persson

Citation: Journal of Applied Physics **119**, 045704 (2016); doi: 10.1063/1.4940700
View online: http://dx.doi.org/10.1063/1.4940700
View Table of Contents: http://aip.scitation.org/toc/jap/119/4
Published by the American Institute of Physics

Understanding the optical properties of $ZnO_{1-x}S_x$ and $ZnO_{1-x}Se_x$ alloys

Gustavo Baldissera[1] and Clas Persson[1,2]
[1]*Department of Materials Science and Engineering, Royal Institute of Technology, SE-100 44 Stockholm, Sweden*
[2]*Department of Physics, University of Oslo, P.O. Box 1048 Blindern, NO-0316 Oslo, Norway*

(Received 18 November 2015; accepted 5 January 2016; published online 28 January 2016)

$ZnO_{1-x}Y_x$ with chalcogen element Y exhibits intriguing optoelectronic properties as the alloying strongly impacts the band-gap energy $E_g(x)$. In this work, we analyze and compare the electronic structures and the dielectric responses of Zn(O,S) and Zn(O,Se) alloys by means of the density functional theory and the partially self-consistent GW approach. We model the crystalline stability from the total energies, and the results indicate that Zn(O,S) is more stable as alloy than Zn(O,Se). We demonstrate also that ion relaxation strongly affects total energies, and that the band-gap bowing depends primarily on local relaxation of the bonds. Moreover, we show that the composition dependent band-gap needs to be analyzed by the band anti-crossing model for small alloying concentration, while the alloying band-bowing model is accurate for strong alloying. We find that the Se-based alloys have a stronger change in the band-gap energy (for instance, $\Delta E_g(0.50) = E_g(\text{ZnO}) - E_g(x = 0.50) \approx 2.2\,\text{eV}$) compared with that of the S-based alloy ($\Delta E_g(0.50) = 1.2\,\text{eV}$), mainly due to a stronger relaxation of the Zn–anion bonds that affects the electronic structure near the band edges. The optical properties of the alloys are discussed in terms of the complex dielectric function $\varepsilon(\omega) = \varepsilon_1(\omega) + i\varepsilon_2(\omega)$ and the absorption coefficient $\alpha(\omega)$. While the large band-gap bowing directly impacts the low-energy absorption spectra, the high-frequency dielectric constant ε_∞ is correlated to the intensity of the dielectric response at energies above 4 eV. Therefore, the dielectric constant is only weakly affected by the non-linear band-gap variation. Despite strong structural relaxation, the high absorption coefficients of the alloys demonstrate that the alloys have well-behaved optoelectronic properties. © *2016 AIP Publishing LLC*.
[http://dx.doi.org/10.1063/1.4940700]

I. INTRODUCTION

Zinc oxide is a rather remarkable semiconductor with a broad variety of material advantages, like for instance, piezoelectricity, high exciton binding energy, and small effective electron mass. Its electronic and optical properties make this oxide capable to be a transparent conductive oxide or an active emitter in optoelectronic devices. ZnO has therefore been subject to extensive research activities. With the advantages of ZnO follow a perseverance to vary and control its materials properties. For instance, it is problematic to *p*-type dope bulk ZnO[1] because compensating native defects are commonly present in the material.[2] Also, tuning in the energy levels of the electronic band edges is crucial for optimizing device performances. For that reason, isovalent ZnO-based cation alloys, such as $(\text{Zn,Cd})\text{O} \equiv \text{Zn}_{1-x}\text{Cd}_x\text{O}$[3,4] are explored, primarily so that the materials properties of the alloys can be varied and still retain some of the advantages of ZnO. By proper isovalent cation alloying the band-gap energy $E_g(x)$ as a function of the alloy composition x can be controlled via the shift of mainly the conduction bands (CBs). Anion alloying within the oxygen family $\text{Zn(O,}Y) \equiv \text{ZnO}_{1-x}Y_x$, on the other hand, can more strongly affect the band edges of both the CBs and the valence bands (VBs), thereby better and more flexible allow tuning the electronic band profile of heterojunction device.

In this article, we analyze the optical properties of the Zn(O,Y) alloys with Y = S and Se. These isovalent alloys are promising for inner layer material in light-emitting diodes or as absorbing material in solar energy applications.[5] We have earlier demonstrated[6] that the Zn(O,S) alloy exhibits a very strong band-gap bowing due to a nonlinear change in both the CB minimum (CBM) and the VB maximum (VBM). This effect in Zn(O,S) has been utilized for activating *p*-type acceptors that are energetically too deep in pure binary ZnO.[7] In this work, we complement the early study by analyzing both the cubic zinc-blende (zb) like phase as well as the hexagonal wurtzite (wz) like phase of the alloy composition, now both for Zn(O,S) and Zn(O,Se). The dielectric function of the Zn(O,Y) alloys are analyzed theoretically by a partially self-consistent Green's function approach. The compositionally dependent crystalline structures, band-gap energy $E_g(x)$, the high-frequency dielectric constant $\varepsilon_\infty(x)$, as well as the optical absorption coefficients are discussed.

We find that the alloys have a strong band-gap bowing where the gap energy reduces from around 3.5 eV for the binaries to about 2.5 for Zn(O,S) and 1.5 eV for Zn(O,Se) with $x = 0.5$. The dielectric constants of ZnO is calculated to be $\varepsilon_\infty = 3.3$, which agrees with the experimental data of 3.7.[8] Interestingly, we find that the composition dependent $\varepsilon_\infty(x)$ of the alloy increases more linearly than expected with respect to x, despite the very strong band-gap bowing. This contradicts the assumption that ε_∞ shall depend inversely on gap energy (i.e., $1/E_g$). From the dielectric functions, the optical absorptions are determined. The absorption coefficient is relatively high near the band-gap energy for all alloy compositions: $\alpha(\omega) > 5 \times 10^4\,\text{cm}^{-1}$ for photon energies

$\hbar\omega > E_g + 1.5\,\text{eV}$. This demonstrates that, even though that it is primarily the states at the band edges that are affected by the alloying, the alloys have mainly delocalized band dispersion without localized defect-like states.

II. COMPUTATIONAL METHODS

The theoretical study of Zn(O,*Y*) is based on a ground-state density functional theory (DFT), employing the projector augmented wave (PAW) basis set as implemented in the VASP package.[9,10] Together with the local density approximation (LDA), we employed the beyond-DFT, quasi-particle GW approximation to verify our DFT results, and also to obtain a better describe the band-gap energy and the optical properties of the materials. We choose the partially self-consistent scGW$_0$ approach,[11] where the Green's functions were iterated until self-consistence was reached while the screened dielectric constant is kept fixed.

We analyze both the hexagonal wurtzite (wz) -like and the cubic zinc-blende (zb) -like structures. For the alloys, we perform scGW$_0$ calculations with 64 (for zb) and 72 (for wz) atom supercells with the alloy composition $x = 0.0$, 0.5, and 1.0 to generate the overall understanding of the alloys. In addition, 300 atom supercells (with $x = 0$, 0.06, 0.13, 0.25, 0.50, 0.75, 0.87, 0.94, and 1.00) are analyzed with the exchange-correlation of LDA. With these supercells, the anion atoms in the alloys were distributed quasi-randomly, avoiding high-symmetry layered structure. (We have seen that layered structures can have similar formation enthalpy as the corresponding quasi-random structures) The binary compounds were fully relaxed (volume and atomic position). The alloys lattice parameters were initially estimated using a linear combination of the relaxed parameters of the binaries, but the atomic positions and the lattice constants were further relaxed with the quasi-Newton algorithm until a maximum force of 8 meV/Å of each atom was reached. The total energy is derived using the LDA calculations. All calculations are performed with a cut-off energy of 300 eV for the regular basis set and 100 eV in the scGW$_0$ part. The scGW$_0$ calculations involve ~500 empty bands. The density is obtained from tetrahedron method integration of the Brillouin zone with a Γ-centered Monkhorst-Pack-like $2 \times 2 \times 2$ **k**-meshes for the scGW$_0$ calculations and $4 \times 4 \times 4$ **k**-meshes for the LDA calculations with large supercells.

In order to compare the band-gap energies and the optical properties of the DFT/LDA calculations (for large supercells) with the scGW$_0$ calculations (for smaller supercells), we also perform LDA+U calculations. Here, one needs a method that can (considering computing time and memory) model large supercells and at the same time calculate response functions that require large **k**-points and many empty bands. At the same time, the method needs to generate sufficiently good gap energies, which is especially important for Zn(O,*Y*) where small alloying content can narrow the gap substantially. We therefore use onsite Coulomb potential correction $U_d(\text{Zn}) = 10\,\text{eV}$ for the Zn *d*-states which improves the states at ~7 eV below VBM, and $U_s(\text{S}) = -6\,\text{eV}$ for the anion *s*-like states to artificially open the energy gap. We understand that applying a correction potential on the *s*- (or *p*-) orbitals can generate incorrect electronic structures (see our earlier study in Ref. 12) and we therefore demonstrate that the chosen parameters in the LDA+U approach roughly describes the optical properties of the Zn(O,*Y*) alloys, although it does involve an inaccuracy of the absorption peaks mainly due to inaccurate dispersion of the CBs.

The analyses of the crystal structures and alloy stability are based on total energy calculations performed by means of the LDA within the DFT. The formation enthalpy ΔH_f of the alloys is calculated based on the electronic total energies E_t per formula unit and the chemical potentials μ_α of the elements α:

$$\Delta H_f(x) = E_t(\text{ZnO}_{1-x}Y_x) - [\mu_{\text{Zn}} + \mu_O \cdot (1-x) + \mu_Y \cdot x]. \tag{1}$$

The chemical potentials $\mu_\alpha = \Delta\mu_\alpha + \mu_\alpha^{ref}$ refer to the solid structures for zinc, sulfur, and selenium, and to the dioxygen molecule for the oxygen. When describing the formation enthalpies, we choose to present the results for the α-rich condition.

In addition to modeling of the heat of formation, we calculate the difference in the total energies between the alloy and its binary constituents for the considered crystalline phase:

$$\Delta E_t(x) = E_t(\text{ZnO}_{1-x}Y_x) - [E_t(\text{ZnO}) \cdot (1-x) + E_t(\text{Zn}Y) \cdot x]. \tag{2}$$

This energy difference describes the energy cost to form the alloy with respect to the more stable binary parts. Although LDA may not accurately describe the absolute values of the total energy due to insufficient exchange-correlation interaction, the calculated energy differences for both ΔH_f and ΔE_t are expected to be more accurate. The reason is that the main errors in absolute values are cancelled out when determining differences in total energies.

The optical properties of the Zn(O,*Y*) alloys are analyzed by the means of the complex dielectric function $\varepsilon(\omega) = \varepsilon_1(\omega) + i\varepsilon_2(\omega)$ and the optical absorption coefficient $\alpha(\omega)$. Here, the dielectric function is calculated from the optical transition probability between the occupied and unoccupied states, subsequently performing the Kramers-Kronig transformation. From the dielectric function the absorption coefficient is directly determined, see References 13 and 14 for details. The dielectric function and absorption spectra are obtained with a Γ-centered $2 \times 2 \times 2$ **k**-mesh for the scGW$_0$ calculations and small unit cells, while $4 \times 4 \times 4$ **k**-mesh for LDA and with the 300 atom supercells.

III. RESULTS

The results from the crystal relaxation of the $\text{Zn(O,}Y\text{)} \equiv \text{ZnO}_{1-x}Y_x$ alloys (Y = S and Se) are presented in Fig. 1 for both the hexagonal wz-like and cubic zb-like phases. The optimized lattice constants are underestimated, as expected from LDA, and the error is 2.5% or less. One notices that the lattice constants of the alloys follow the

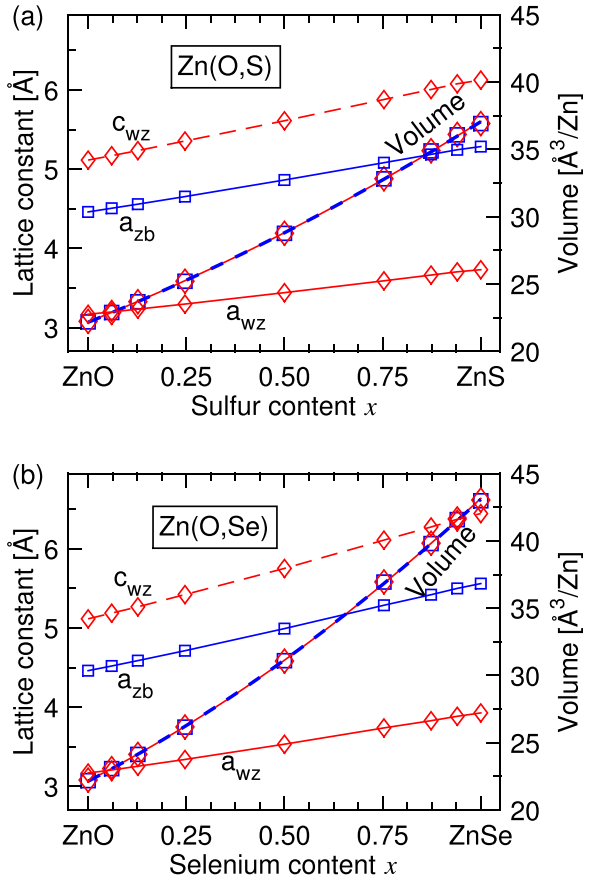

FIG. 1. The lattice constants (left axis) and unit cell volume (right axis) of wurtzite-like (diamond marks) and zinc-blende-like (square marks) of the $Zn(O,Y) \equiv ZnO_{1-x}Y_x \equiv Zn(O,Y)$ alloy with (a) $Y = S$ and (b) $Y = Se$. The zb-like structures have only slightly smaller volumes than the corresponded wz-like structure for the same anion composition.

Vegard's law with a fairly linear increase with respect to sulfur or selenium content x; the maximum deviation from a linear behavior is 0.3% for Zn(O,S) and 0.5% for Zn(O,Se). This well-behaved change in the lattice parameters for the alloy is because the relaxation implies minor structural changes of the atom sites from the ideal wz and zb phases.

The relaxation with distortion of the crystalline structure is driven by the attempt to retain proper bonds and bond length as much as possible. That is, since the covalent radii for tetrahedral bonds of Zn, O, S, and Se are 1.30, 0.67, 1.04, and 1.14 Å[15] the preferred, ideal covalent bond lengths are 1.97, 2.34, and 2.44 Å for the Zn–O, Zn–S, and Zn–Se bonds, respectively. From Tables I and II, one observes that the calculated bond lengths for the binary compounds (δ(Zn–O) = 1.93 Å for ZnO, δ(Zn–S) = 2.29 Å for ZnS, and δ(Zn–Se) = 2.41 Å for ZnSe) are close to the ideal lengths and the deviation is at most ~2% (for ZnO) which again reflects that LDA tends to overbind by about 2%–3%. Moreover, for the alloys the bond lengths of Zn–O, Zn–S, and Zn–Se are rather stable (within a 3%–5% change for the considered structures) even though that the lattice constants change by about 13%–15% for Zn(O,S) and 18%–19% for Zn(O,Se). Here, the Zn(O,Se) alloys have the largest variation of the bond lengths, and the change of the Zn–O bonds is 1%–2% larger than the corresponding change of the Zn–Y bonds.

The volume increases about 66% from ZnO to ZnS and about 94% from ZnO to ZnSe, thus ZnSe has almost twice as large cell volume as ZnO. Since both phases have tetrahedral local geometry the cell volumes of the wz and the zb Zn(O,Y) structures are very similar; the largest difference in volume is for ZnO where the zb phase is 0.2% smaller than the wz phase. This is further verified by converting the cubic lattice parameter a_{zb} to the corresponding hexagonal parameters: $a_{wz\leftarrow zb} = a_{zb}/\sqrt{2}$ and $c_{wz\leftarrow zb} = 2a_{zb}/\sqrt{3}$. The difference between $a_{wz\leftarrow zb}$ for zb-ZnO and a_{wz} for wz-ZnO is 0.7%, while the corresponding difference between zb- and wz-like Zn(O,Y) alloys with $x = 0.5$ is almost 0%. For the hexagonal phase, the ratio c_{wz}/a_{wz} is somewhat constant for the alloys. The ratio is between 1.61 and 1.64 for both Zn(O,S) and Zn(O,Se) which is close to the ideal value of 1.63 for wz structures. $c_{wz}/a_{wz} \approx 1.61$ for ZnO, and the ratio is increasing for larger Y content with $c_{wz}/a_{wz} \approx 1.64$ for both ZnS and ZnSe. ZnO with a large electronegativity of the oxygen atom (about 3.44[19]) has stronger long-range polar interactions along the c-direction than ZnS and ZnSe (with anion electronegativity 2.58 and 2.55, respectively) and that is reflected in the c_{wz}/a_{wz} ratio. The small value of c_{wz}/a_{wz} for ZnO partly explains the resistance of the compound to be formed in a cubic structure. Alloying with S or Se, the ratio c_{wz}/a_{wz} increases to the ideal value for composition around $x \approx 0.5$–0.7 which is also roughly the composition for which the formation enthalpy of the zb phase becomes smaller than of the corresponding wz phase. The difference in ΔH_f between the wz and zb phases is about −20 meV/Zn for ZnO (wz phase is more stable) and about 8 and 10 meV/Zn for ZnS and ZnSe, respectively (thus, zb more stable). This may indicate mixed phases, phase transition, or even crystal structure instability for alloys with composition $x \approx 0.5$–0.7. Synthesis and experimental characterizations support this. For instance, reported X-ray diffractograms of Zn(O,S) show single wz-like phase for $x = 0$, 0.10, 0.28, 0.84, and 0.97, whereas the $x = 0.48$ sample has a weak crystalline structure on amorphous background and $x = 0.71$ sample is completely amorphous.[6] Other experimental studies report stable Zn(O,S) alloys with crystalline morphology for different ranges of composition, depending on the growing technique used and treating of the samples.[20–24]

The calculated absolute values of the formation enthalpies for wz-ZnO and wz-ZnS are $\Delta H_f = -3.65$ and −1.75 eV, respectively (Fig. 2), which agree well with the measured data −3.63 and −1.99 eV.[13,16] Here, our calculated reference chemical potentials μ_α^{ref} from LDA are −1.86, −5.24, −4.56, and −3.86 for Zn, O, S, and Se, respectively. Using different values of the reference chemical potentials changes the formation enthalpy, but the qualitative results remain the same. Also, the calculated ΔH_f for zb ZnS and ZnSe (−1.75 and −1.39 eV/Zn, respectively) agree rather well with experimental data (−2.13 and −1.65 eV/Zn, respectively); however, it is less comparable than for wz-ZnO. This deviation can of course be due to our computational approach and chemical potentials and also due to the noninclusion of phonon contributions, and a possible variation of the energy in the other allotropes is not included for S and Se, despite several allotropes were calculated. One

TABLE I. The formation enthalpy ΔH_f of the $ZnO_{1-x}S_x$ alloy per formula unit refers to the $\Delta\mu_\alpha = 0$ condition. The total energy difference ΔE_t refers to the total energies of the ZnO and ZnS binaries with the phase as the considered alloy. The average bond lengths δ(Zn–O) ≈ 1.9–2.0 Å and δ(Zn–S) ≈ 2.2–2.3 Å are relatively constant for the different alloy compositions; the standard deviation is also shown. $a_{wz\leftarrow zb}$ and $c_{wz\leftarrow zb}$ are the equivalent lattice parameters for an ideal wz structure based on the zb lattice parameter a_{zb}; notice the small difference of these values for zb structure compared with the actual wz structure.

	$ZnO_{1-x}S_x$					Expt.	
	$x = 0.00$	0.25	0.50	0.75	1.00	ZnO	ZnS
Hexagonal wz-like structure							
ΔH_f [eV/Zn]	−3.65	−3.04	−2.52	−2.09	−1.75	−3.63[a]	−1.99[b]
ΔE_t [eV/Zn]	0	0.14	0.18	0.13	0		
a_{wz} [Å]	3.17	3.30	3.44	3.59	3.74	3.25[c]	3.82[c]
c_{wz} [Å]	5.12	5.35	5.61	5.88	6.13	5.20[c]	6.26[c]
δ(Zn–O) [Å]	1.93 ± 0.00	1.96 ± 0.02	1.98 ± 0.03	2.00 ± 0.03		1.98[d]	
δ(Zn–S) [Å]		2.23 ± 0.02	2.26 ± 0.02	2.27 ± 0.02	2.29 ± 0.00		2.34[d]
Cubic zb-like structure							
ΔH_f [eV/Zn]	−3.63	−3.03	−2.52	−2.09	−1.75		−2.13[b]
ΔE_t [eV/Zn]	0	0.14	0.17	0.13	0		
a_{zb} [Å]	4.46	4.65	4.86	5.08	5.29	4.60[e]	5.41[c]
$a_{wz\leftarrow zb}$ [Å]	3.15	3.29	3.44	3.59	3.74	3.25	3.82
$c_{wz\leftarrow zb}$ [Å]	5.15	5.37	5.62	5.87	6.10	5.31	6.24
δ(Zn–O) [Å]	1.93 ± 0.00	1.96 ± 0.02	1.98 ± 0.02	2.00 ± 0.03		1.99[d]	
δ(Zn–S) [Å]		2.23 ± 0.02	2.26 ± 0.02	2.28 ± 0.02	2.29 ± 0.00		2.34[d]

[a]Madelung *et al*. (expt.), Ref. 13.
[b]Mills (expt.), Ref. 16.
[c]Madelung (expt.), Ref. 8.
[d]Values obtained from the respective cells parameters, considering equal nearest-neighbor bond lengths.
[e]Kim *et al*. (expt.), Ref. 17.

notices that the formation enthalpy goes fairly linearly with respect to the sulfur content, and that the formation enthalpies of the wz and the zb phases are almost equal. The difference in the formation energies between the wz and zb phases is small. For binary ZnO, the difference is only ∼20 meV per Zn atom where the wz phase has the lowest energy, whereas for binary ZnS the zb phase has the lowest energy with the difference of ∼8 meV/Zn. For the Zn(O,S) alloy, the difference increases somewhat and for about 60% sulfur content the two phases have equal formation enthalpy. Although

TABLE II. Same as Table I, but for $ZnO_{1-x}Se_x$.

	$ZnO_{1-x}Se_x$					Expt.	
	$x = 0.00$	0.25	0.50	0.75	1.00	ZnO	ZnSe
Hexagonal wz-like structures							
ΔH_f [eV/Zn]	−3.65	−2.86	−2.23	−1.75	−1.38	−3.63[a]	
ΔE_t [eV/Zn]	0	0.23	0.28	0.19	0		
a_{wz} [Å]	3.17	3.34	3.53	3.74	3.93	3.25[b]	4.00[c]
c_{wz} [Å]	5.12	5.42	5.75	6.11	6.44	5.20[b]	6.54[c]
δ(Zn–O) [Å]	1.93 ± 0.00	1.97 ± 0.03	2.00 ± 0.04	2.02 ± 0.21[d]		1.98[e]	
δ(Zn–Se) [Å]		2.34 ± 0.03	2.37 ± 0.04	2.39 ± 0.03	2.41 ± 0.00		2.45[e]
Cubic zb-like structures							
ΔH_f [eV/Zn]	−3.63	−2.86	−2.22	−1.74	−1.39		−1. 65[f]
ΔE_t [eV/Zn]	0	0.21	0.28	0.20	0		
a_{zb} [Å]	4.46	4.71	4.99	5.29	5.56	4.60[g]	5.67[b]
$a_{wz\leftarrow zb}$ [Å]	3.15	3.33	3.53	3.74	3.93	3.25	4.01
$c_{wz\leftarrow zb}$ [Å]	5.15	5.44	5.76	6.10	6.42	5.31	6.54
δ(Zn–O) [Å]	1.93 ± 0.00	1.97 ± 0.02	2.00 ± 0.04	2.03 ± 0.23[d]		1.99[e]	
δ(Zn–Se) [Å]		2.34 ± 0.02	2.37 ± 0.04	2.39 ± 0.04	2.41 ± 0.00		2.45[e]

[a]Madelung *et al*. (expt.), Ref. 13.
[b]Madelung (expt.), Ref. 8.
[c]Villars *et al*. (expt.), Ref. 18
[d]Two atomic bonds were dissociated in each of these compounds due to extensive structural changes; the total bond length ∼4Å. The statistic is calculated considering the bond length of these broken bonds. Without this, the standard deviation would be in the same range of the other compounds.
[e]Values obtained from the respective cells parameters, considering equal nearest-neighbor bond lengths.
[f]Mills (expt.), Ref. 16.
[g]Kim *et al*. (expt.), Ref. 17.

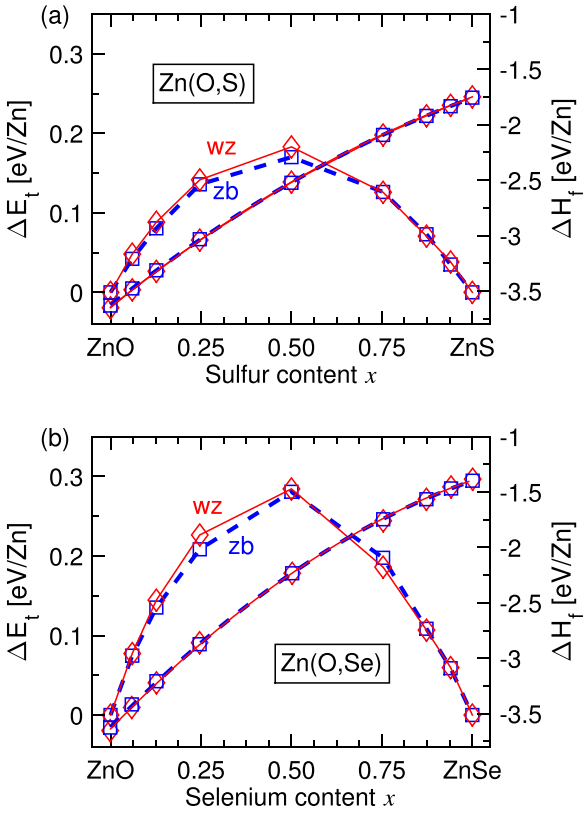

FIG. 2. The energies ΔE_t and ΔH_f (in units of eV per Zn atom) for wz-like (red diamond marks) and zb-like (blue squared marks) phases of (a) Zn(O,S) and (b) Zn(O,Se). The energy ΔE_t is calculated from the energy difference with respect to the binary compounds. The formation energy ΔH_f indicates that the hexagonal structure is the most stable phase for alloying content $x < 0.5$.

more detailed theoretical investigation is needed to analyze the phase stabilities and crystalline imperfections, the theoretical results indicate that alloys with high crystalline morphology can be formed. Moreover, below (above) the breaking point at $x \approx 0.5$–0.8 the wz (zb) phase is most stable, and mixed phases are expected in the region around this breaking point.

To further analyze the crystal stability of the Zn(O,Y) alloys, we present in Fig. 2 the total energy difference ΔE_t which describes the energy required to form the alloys with respect to the binary constituents. This is an estimate of the occurrence of precipitation of binary phase in the materials. The energy difference reaches its maximum at $x \approx 0.5$ as expected, and the value of ΔE_t is reasonable for alloys:[25] we obtain $\Delta E_t(x = 0.5) = 0.18$ eV/Zn for Zn(O,S) and 0.28 eV/Zn for Zn(O,Se). Zn(O,Se) has 50% larger energy difference compared with Zn(O,S) indicating a less crystalline stable alloy. In addition to that, the formation enthalpy ΔH_f of ZnSe is about 0.4 eV/Zn larger than that of ZnS, and the difference in anion atom sizes between Se and O is 0.12 Å larger than that between S and O. This also indicates that Se-based alloys are less easy to synthesize than the S-based alloys. This may also explain why Pan *et al.*[26] found that the amorphous state $Zn_xSe_{1-x}O_2$ is easier to form and compare with the formation of O doped $ZnSe_{1-x}O_x$ alloy.

Although the wz-like phase has typically ~10 meV/Zn smaller formation enthalpy, the energy difference in the zb alloy is smaller than the wz phase though this difference is only at most ~15 meV/Zn. The energy difference does, however, not describe that the zb phase is more stable than the wz phase, instead it only compares the total energy of the zb-like alloy (or wz-like alloy) with respect to the total energies of zb phase (or wz phase) of the binaries, and thus not with respect to a common reference system. Overall, however, the results suggest that there is a possibility to form crystalline Zn(O,Y) alloys with random configuration, especially for Zn(O,S), although single-phase might be difficult to obtain in the region $x \approx 0.5$–0.8.

Although the crystalline lattice parameters change fairly linearly with respect to the sulfur or selenium content, the

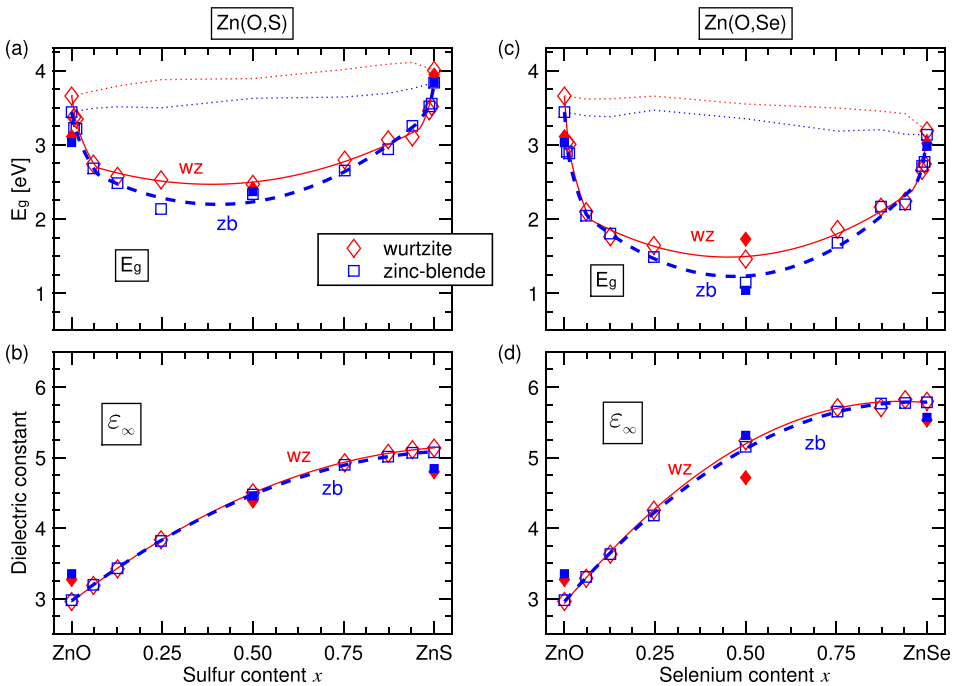

FIG. 3. The band-gap energy E_g in (a) Zn(O,S) and (c) Zn(O,Se) depends strongly on the alloy composition. Open marks show the LDA+U results and the filled marks for $x = 0$, 0.5, and 1 are the scGW$_0$ results. The parameters describing the gap-energy variation (solid and dashed lines) are given in the main text. The corresponding gap energies for unrelaxed structures (dotted lines) exhibit fairly linear dependence with respect to composition. The high frequency dielectric constant ε_∞ for Zn(O,S) and Zn(O,Se) indicates that the cubic and hexagonal phases have very comparable optical properties. Since the anisotropy between the transverse and the longitudinal components of ε_∞ is relatively small in the wz structures (see Table III), we present in this figure the geometric average value of the two components.

fundamental band-gap of Zn(O,*Y*) exhibits a strong gap narrowing [Figs. 3(a) and 3(c)]. Compared with the band-gap energy of ZnO, the energy gaps of the alloys are decreased by ∼1.2 eV for wz-like Zn(O,S) and ∼2.2 eV for Zn(O,Se) at the composition $x = 0.5$. The zb-like alloys have a similar band-gap narrowing. We have found that small variations in the anion configuration, i.e., the distribution of oxygen and sulfur atoms, have a relatively large impact on the gap energies (within 0.1–0.3 eV) and that explains the somewhat uncertainty of the energies in the figure. Nevertheless, we conclude that the Se-based alloy has thus roughly twice as large shift of the gap energy as the S-based alloy, and the band-gap decreases to a value around 1.5 eV for $ZnO_{0.5}Se_{0.5}$. That implies an energy gap that is very suitable for solar energy technologies. Moreover, since the change in band-gap energy is rather similar for wz- and zb-like phases, mixed phase alloys (e.g., in the region $x \approx 0.5$–0.8) is less problematic for achieving a functional material.

One observes that the change in the band-gap is largest for small x and also for very large x. Thus, the variation in the gap energy can be divided into three regions: region 1 at small x which can be described as ZnO-like host material doped or modestly alloyed with Y, region 2 where Zn(O,Y) is a well-behaved alloy of the ZnO and ZnY constituents, and region 3 which is ZnY-like host material doped or modestly alloyed with O. The change in the energy gap has been described by the band anti-cross (BAC) model[27–29] or by the alloy band bowing (ABB) model,[23,24,30] where the latter model sometimes is extended with an additional analytic function for better fitting. Here, we suggest combining the two models. That is, to use the BAC model in order to describes weakly doped/alloyed materials (regions 1 and 3) where the host materials are only perturbed by the doping/alloying, whereas to use the regular ABB model to describe the highly doped/alloyed materials (region 2) where the alloys has a more compound-like behavior. The combined model of the band-gap energies is thereby described as:

$$\begin{aligned} E_g(x) &= \frac{1}{2}\left(E_g(\mathrm{ZnO}) + E_{a0} - \sqrt{\left(E_g(\mathrm{ZnO}) - E_{a0}\right)^2 + 4V_0^2 \cdot x}\right) && \text{for regions 1,} \\ E_g(x) &= E_{b0} \cdot (1-x) + E_{b1} \cdot x - b \cdot x(1-x) && \text{for region 2, and} \\ E_g(x) &= \frac{1}{2}\left(E_g(\mathrm{ZnY}) + E_{a1} - \sqrt{\left(E_g(\mathrm{ZnY}) - E_{a1}\right)^2 + 4V_1^2 \cdot (1-x)}\right) && \text{for regions 3.} \end{aligned} \tag{3}$$

We fit the calculate gap energies for the whole composition range $0 \le x \le 1$ to the expressions for the three regions. The resulting parameters for wz-like Zn(O,S) are $E_{a0} = 3.94$, $V_0 = 4.24$, $E_{b0} = 2.80$, $E_{b1} = 3.32$, $b = 2.26$, $E_{a1} = 3.93$, and $V_1 = 3.82$ in units of eV. The corresponding values for zb-like Zn(O,S) are $E_{a0} = 3.91$, $V_0 = 3.91$, $E_{b0} = 2.78$, $E_{b1} = 3.48$, $b = 3.61$, $E_{a1} = 3.80$, and $V_1 = 2.44$. Zn(O,Se) has larger change in the band-gap energies, and the resulting parameters for wz-like Zn(O,Se) are $E_{a0} = 3.65$, $V_0 = 6.31$, $E_{b0} = 2.20$, $E_{b1} = 2.53$, $b = 3.47$, $E_{a1} = 3.14$, and $V_1 = 3.99$, and the corresponding values for zb-like Zn(O,Se) are $E_{a0} = 3.44$, $V_0 = 5.61$, $E_{b0} = 2.30$, $E_{b1} = 2.62$, $b = 4.91$, $E_{a1} = 3.13$, and $V_1 = 3.82$. The resulting fitted curves are displayed as solid and dashed lines in Figs. 3(a) and 3(c). The approximate boundary for regions 1 and 2 is about $x_{12} = 0.06$ for all considered alloys, and the corresponding boundary for regions 2 and 3 is about $x_{23} = 0.96$.

The uncertainty in the fitting of Eq. (3) to the gap energies is dominated by the variation of the calculated band gap energies. The maximum energy deviation of the calculated gap energies and the fitted curves in region 1 (doping region) is 0.06 eV for Zn(O,S) and 0.10 eV for Zn(O,Se) alloys. Corresponding deviation in region 3 (also doping region) is 0.13 and 0.10 eV, while the deviation in region 2 (alloying region) is 0.15 and 0.13 eV, respectively. Not surprisingly, the largest uncertainty is thus for Zn(O,S) alloy and region 2. One reason for deviation is not having perfectly an alloy system that is infinitely large and with perfectly random distribution of the anion atoms. Using large supercells with 300 atoms, one can generate fairly quasi-random distributions; however, different atomic configurations will have varying degree of ordering of the two anion types.

To justify the utilization of a combined the BAC and ABB models, we plot in Fig. 4 the atomic-resolved local density-of-states (LDOS) of wz-like Zn(O,Se). For modest alloying [here, $x \le x_{12} = 0.07$; region 1; Fig. 4(a)], it is clear that Se *p*-like states are distributed at the very top of the VBs. The O *p*-like states are more disperse and actually is very close to the corresponding states for pure ZnO. Thus, the ZnO-like LDOS is (almost) not affected by the alloying, and a perturbative approach is suitable. At the other limit [here, $x \ge x_{23} = 0.96$; region 3; Fig. 4(c)] similar thing is seen, that is, the ZnSe-like LDOS is (almost) not affected by the alloying. For alloying in the intermediate region [here, $0.07 \le x \le 0.96$; region 2; Fig. 4(b)] both the O *p*-like states and the Se *p*-like states are more hybridized over the whole VB region, and here the alloying model is therefore more appropriate.

Thus, substituting the anion changes significantly the band-edge properties with only a moderate change in the crystalline structure. It is well known that heavily doping of traditional semiconductors reduces the fundamental band-gap energy,[31] but in that case it is the free carrier concentration in conjunction with charged dopants that cause the narrowing of the gap. The Zn(O,*Y*) alloys involve an isovalent alloying configuration that does not generate free carriers, and thus the

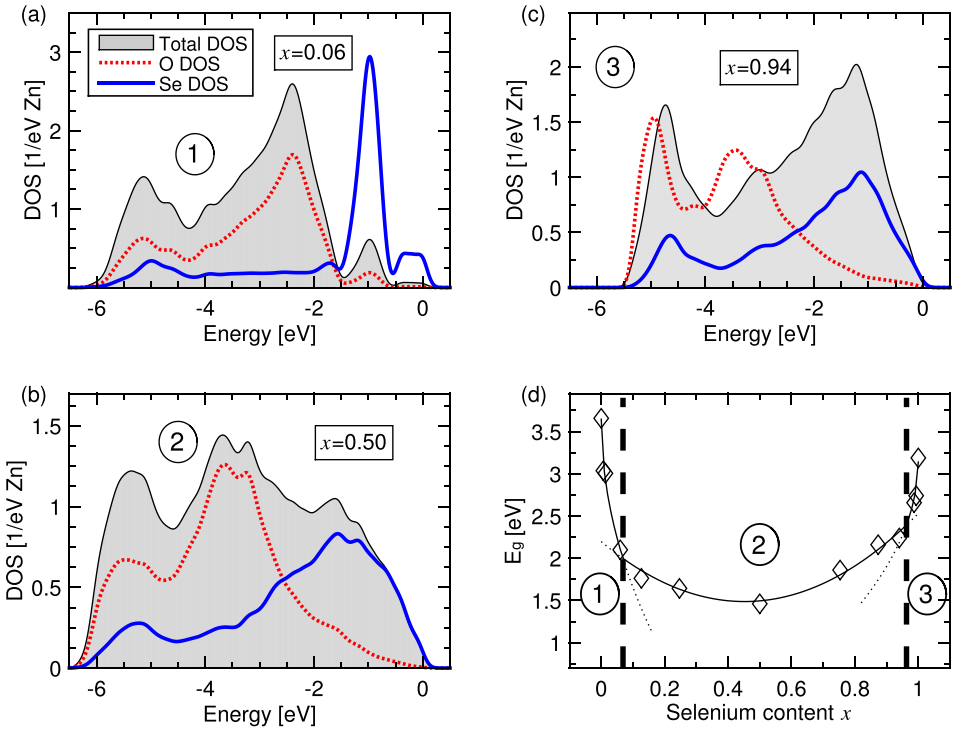

FIG. 4. Atomic-resolved LDOS of wz-like Zn(O,Se) for (a) $x=0.06$, (c) $x=0.50$, (b) $x=0.94$, from the LDA+U calculation. The energy refers to the VBM and the LDOS is presented with a 0.1 eV Lorentzian broadening. The subfigure (d) shows the band-gap energy of the alloy over the whole compositional range (diamond marks and the fitted solid line). The two dashed vertical lines indicate the approximate boundaries for the three regions, described by the band anticrossing model (in regions 1 and 3) for dilute alloying, and the alloy band bowing model (in region 2) for strong alloying. The dotted lines in (d) follow the contour of the solid lines, to demonstrate the results of the models outside their corresponding regions.

alloy is still a semiconductor. Instead, in Zn(O,*Y*) the underlying reasons for the band-gap narrowing are twofold: First, the S 3*p* and Se 4*p* states are energetically higher located than the O 2*p* states. Therefore, substituting oxygen by sulfur or selenium in the Zn(O,*Y*) alloy shifts the anion-like VBM upwards and the band-gap is decreased. For high alloying content ($x>0.5$), the CBM is increased whereas the VBM is more stable, and the band-gap is thereby increased again. We have found the same type of effect on the gap narrowing in ZnO–GaN and ZnO–InN alloys, where N substituting O has similar effect on the VBM.[32] Second, the ion relaxation forms covalent bonds which tends to preserve the bonds lengths and that have an impact on both the energy levels of the *p*-like states and the O–*Y* hybridization. In Fig. 3, we present the band-gap energies for unrelaxed structure, that is, hypothetical structures with ideal positions of the atoms but with relaxed volume. Here, the bond lengths of Zn–O and Zn–*Y* will thus be equal for each specific composition *x*. The relaxed volume are however very similar to the volume of the corresponding true alloy. With these unrelaxed structures, we find that the band-gap increases roughly linearly with respect to an increased alloy composition *x*. The unrelaxed structures are of course rather unrealistic structures, and the energy gain for atom relaxation to the ground-state configuration is very large: ∼2.0 eV/Zn for wz-Zn(O,S) and ∼2.3 eV/Zn for wz-Zn(O,Se) for $x=0.50$. However, this hypothetic modeling demonstrates that the atomic relaxation to preservation of covalent bond lengths has a major role for the gap narrowing.

The energy levels of anion *p*-like states, the atom sizes, and the covalent bond lengths depend on each other. They explain together the band-gap narrowing in the Zn(O,*Y*) alloys. This strong band-gap narrowing for about 5%–15% alloying content can be utilized to tune and optimize the band-edge profile of devices, and even enhance dopability by activating otherwise too localized acceptor states.[6,7]

The optical responses of the Zn(O,*Y*) alloys are analyzed in terms of the complex dielectric function $\varepsilon(\omega)=\varepsilon_1(\omega)+i\varepsilon_2(\omega)$. Figure 5 presents the results for wz-like Zn(O,S); however, the other three considered alloys have all qualitatively the same dielectric responses; see supplementary material.[33] Both the real part $\varepsilon_1(\omega)$ and the imaginary part $\varepsilon_2(\omega)$ of the dielectric function change rather smoothly with respect to sulfur content. The real part of the dielectric function increases monotonically in the energy range $0\le\hbar\omega\le\sim5$ eV as a function of the energy. In the energy region 4–6 eV, the $\varepsilon_1(\omega)$ increases considerably with increasing sulfur content. Also the peak at 5–7 eV in $\varepsilon_2(\omega)$ increases substantially with increasing sulfur content. Thus, for those parts of the dielectric function, the band-gap narrowing of the alloy has less impact on the dielectric response. In the low energy region, however, $\varepsilon_2(\omega)$ depends more on the electronic band-gap energy [see inset of Fig. 5(b)], and in the energy region $\hbar\omega\le\sim4$ eV the alloys with smallest gap energies have the largest imaginary part; this will thus affect the optical absorption of the alloys for the low-energy photons.

The high-frequency dielectric constant ε_∞ is determined (Table III) from the dielectric response $\varepsilon_1(\omega)$ at zero frequency and neglecting the ionic contribution. The calculated values tend to be somewhat smaller than the available measured data. The theoretical data is determined as zero-temperature values and neglecting contribution from the small polaron coupling, whereas the experimental measurements are at room temperature. This might partly explain the smaller calculated values. A minor part of this discrepancy is explained that we calculate the values $\varepsilon_\infty=\varepsilon_1(\omega=0)$ at zero frequency when electron-phonon interaction is neglected, while the measured values are obtained within the energy

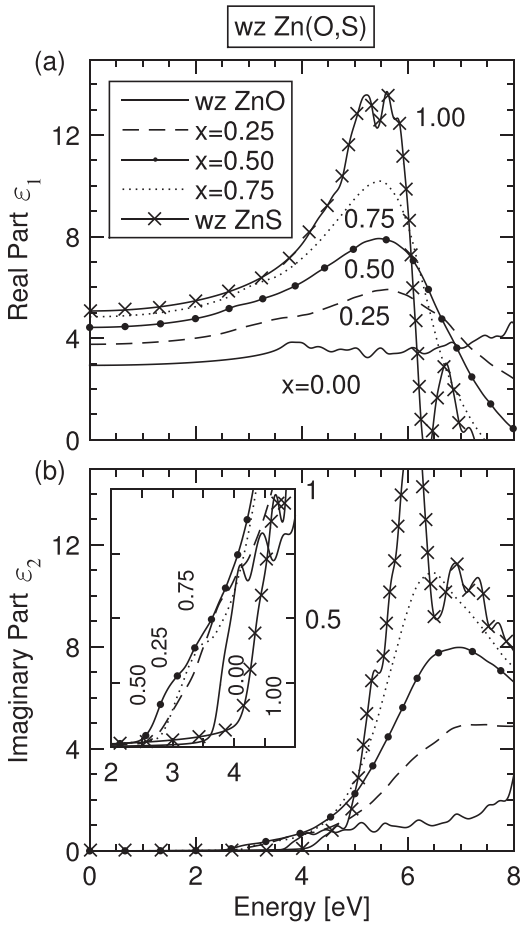

FIG. 5. Dielectric function $\varepsilon(\omega)$ of wz-like Zn(O,S) for $x=0$ (ZnO; solid lines), $x=0.25$ (dashed lines), $x=0.50$ (lines with large dots), $x=0.75$ (dotted lines), and $x=1$ (ZnS; lines with crosses). The inset figure shows a close-up at the band-edge energies. We present the isotropic geometric average value because the anisotropy is small (see Table III), and the spectra include a 0.05 eV Lorentzian broadening. The zb- and wz-like phases of Zn(O,S) and Zn(O,Se) have all rather similar spectra of their dielectric responses, see supplementary material.[33]

region $0<\omega<E_g/\hbar$. Since the real part of the dielectric function increases in this energy, the experiments will measure a larger value. The calculated $\varepsilon_\infty=\varepsilon_1(\omega=0)$ of the binary wz-ZnO, zb-ZnS, and zb-ZnSe are $\varepsilon_\infty=2.9$, 5.1, and 5.8 from LDA+U and 3.3, 4.8, and 5.6 from scGW$_0$, respectively; here, we present the average value for the anisotropic wz-ZnO. The calculated mid-gap values of the real part of the dielectric function are $\varepsilon_1(\omega\approx 0.5\cdot E_g/\hbar)=3.0$, 5.4, and 6.2 for wz-ZnO, zb-ZnS, and zb-ZnSe from LDA+U and 3.3, 5.1, and 5.8 from scGW$_0$, respectively. The values at the band-gap energy $\varepsilon_1(\omega\approx E_g/\hbar)=3.71$, 7.3, and 8.2 from LDA+U and 3.62, 6.05, and 6.7 from scGW$_0$. The corresponding experimental results from the ellipsometry spectroscopy measurements are $\varepsilon_\infty=3.7$, 5.1, and 5.7, respectively.[8] Considering the uncertainty in both theoretical and experimental data, the trends in the dielectric constants agree overall fairly well between the theoretical and experimental findings.

The static dielectric constant ε_0 is determined by means of the Born effective charges and using the LDA potential.[36] This is thus the dynamic effective charges which models the electron-optical phonon interaction. The calculated static dielectric constants of binary wz-ZnO, zb-ZnS, and zb-ZnSe are $\varepsilon_0=7.6$, 7.5, and 8.1, respectively. The corresponding experimental values are $\varepsilon_0=\varepsilon_1(\omega\approx 0)=8.7$, 8.3, and 8.6, respectively.[8] Our calculated values are thus slightly underestimated. For wz-like Zn(O,S), we find that the geometric average values change as $\varepsilon_0=7.6$, 8. 7, and 7.4 for $x=0.0$, 0.5, and 1.0, respectively. wz-like Zn(O,Se) has a similar behavior: $\varepsilon_0=7.6$, 10.0, and 8.6, respectively. The static dielectric constant $\varepsilon_0(x)$ depends on the local ionicity of the compound elements. Therefore, the change in the crystal structure by relaxation of the Zn(O,*Y*) alloys generates a local charge distribution that affects the Born effective charges. Thereby, $\varepsilon_0(x)$ depends on the oxygen content, and it has a maximum value at about $x\approx 0.50$.

Intriguingly, the high-frequency dielectric constant $\varepsilon_\infty(x)$ increases somewhat linearly as a function of the alloying content x (Fig. 3). This is opposite to what is expected because the high-frequency dielectric constant is related to the band-gap energy (while the static dielectric constant ε_0 is related to the ionicity of the compound). Thus, one would expect that the high-frequency dielectric constant follows inversely the change in $E_g(x)$. The reason for not doing so fully, and instead having a more linear behavior $\varepsilon_\infty(x)$ is due to the difference in the imaginary part of the dielectric function $\varepsilon_2(\omega)$ in the energy region above ~4 eV, see Fig. 5. The high-frequency dielectric constant is obtained from the Kramers-Kronig transformation relation by integrating $\varepsilon_2(\omega)$ from the energy 0 to infinity. Thus, ε_∞ depends both on the gap energy and the shape of $\varepsilon_2(\omega)$ for the higher energy region. In the case of the Zn(O,S) alloys, the sulfur rich alloys have strong peak in $\varepsilon_2(\omega)$ at about 5–7 eV (see Fig. 5) and this peak increases with respect to the alloying content. In wz-like Zn(O,S), the maximum value of the sharp peak is $\varepsilon_2(\omega\approx 6\text{–}8\,\text{eV})\approx 3.5$, 5.0, 8.0, 10.9, and 17.3 for $x=0$, 0.25, 0.50, 0.75, and 1.0; thus a somewhat linear increase. Also, the main peak in $\varepsilon_1(\omega)$ at around 5 eV goes fairly linearly.

In order to better understand how $\varepsilon_2(\omega)$ affects the value of ε_∞, we analyze wz-like Zn(O,S) alloys for different conditions (Fig. 6). The solid line in the figure is the correct $\varepsilon_\infty(x)$ for wz-like Zn(O,S) which increases somewhat linearly with a moderate bowing; this is thus the same results as in Fig. 3. The dashed line represents the corresponding $\varepsilon_\infty(x)$ for unrelaxed structures, that is, structures with ideal positions of the atoms in the wz structure. For the unrelaxed structures, a more linear behavior is obvious. This agrees with the results that the unrelaxed alloys do not exhibit any band-gap narrowing and instead $E_g(x)$ goes linearly with respect to x (see Fig. 3). Next, we want to show that $\varepsilon_\infty(x)\propto 1/E_g(\mathrm{x})$ for an ideal case, and we therefore start with the imaginary part of the dielectric function $\varepsilon_2(\omega)$ of binary wz-ZnO. We then model ε_∞ from a hypothetic wz-ZnO compounds for which the band-gap E_g can be varied. That is, we calculate the value of $\varepsilon_\infty(x)$ from that $\varepsilon_2(\omega)$ but where the dielectric function of wz-ZnO has been shifted on the energy scale to have the same onset to response as the electronic band-gap of the wz-like Zn(O,S). Thus, the Kramers-Kronig transformation is performed for $\varepsilon_2(\omega+(E_g(x)-E_g(\mathrm{ZnO}))/\hbar)$. This simulates that a hypothetic material that has different gap energies, i.e.,

TABLE III. The fundamental band-gap energy E_g is for the direct Γ-point energy gap. The high-frequency ε_∞ dielectric constants are presented the wz-like structures for the transverse ⊥ and longitudinal || components. We compare data from our LDA+U, scGW$_0$ calculations and earlier published calculations or measurements.

	$ZnO_{1-x}Y_x$									
	$x = 0.00$ (ZnO)			0.25	0.50		0.75	1.00 (Zn*Y*)		
wz-like $ZnO_{1-x}S_x$	LDA+U	scGW$_0$	Other	LDA+U	LDA+U	scGW$_0$	LDA+U	LDA+U	scGW$_0$	Other
E_g [eV]	3.66	3.11	3.44[a]	2.53	2.47	2.41	2.79	4.00	3.94	3.91[a]
$\varepsilon_\infty^\perp$	2.9	3.2	3.70[a]	3.7	4.4	4.4	4.8	5.0	4.75	5.61[b]
$\varepsilon_\infty^{\|\|}$	3.0	3.3	3.75[a]	3.8	4.5	4.5	4.9	5.1	4.90	5.91[b]
zb-like $ZnO_{1-x}S_x$										
E_g [eV]	3.44	3.03	3.28[c]	2.14	2.34	2.37	2.65	3.84	3.84	3.72[a]
ε_∞	3.0	3.4	5.1[d]	3.8	4.5	4.5	4.9	5.1	4.84	5.2[e]
wz-like $ZnO_{1-x}Se_x$										
E_g [eV]	3.66	3.11	3.44[a]	1.64	1.46	1.73	1.86	3.19	3.02	2.80[e]
$\varepsilon_\infty^\perp$	2.9	3.2	3.70[a]	4.1	5.1	4.6	5.6	5.7	5.47	
$\varepsilon_\infty^{\|\|}$	3.0	3.3	3.75[a]	4.3	5.2	4.8	5.7	5.8	5.66	
zb-like $ZnO_{1-x}Se_x$										
E_g [eV]	3.44	3.03	3.28[c]	1.49	1.14	1.04	1.68	3.13	2.98	2.82[a]
ε_∞	3.0	3.4	5.1[d]	4.2	5.2	5.3	5.6	5.8	5.57	5.7[a]

[a]Madelung (expt.), Ref. 8.
[b]Kootstra *et al*. (theory), Ref. 34.
[c]Kim *et al*. (expt.), Ref. 17.
[d]Serrano *et al*. (theory), Ref. 35.
[e]Madelung *et al*. (expt.), Ref. 13.

the same $E_g(x)$ as the Zn(O,S) alloys. With this hypothetic material, the $\varepsilon_\infty(x)$ is proportional to $1/E_g(x)$; see lower dashed-dotted line with cross marks in Fig. 6. Correspondingly, we also calculate the value of $\varepsilon_\infty(x)$ from the dielectric function of binary wz-ZnS, which also shifted to have the same band-gap energy as the alloy, thus from $\varepsilon_2(\omega + (E_g(x) - E_g(\mathrm{ZnS}))/\hbar)$ using $\varepsilon_2(\omega)$ of wz-ZnS, see dashed-dotted line with plus marks in the figure. Also here

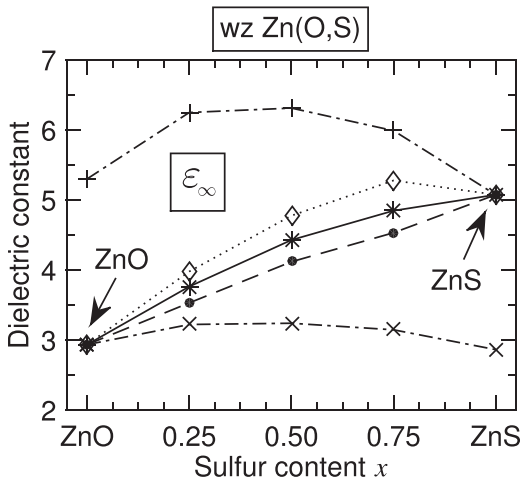

FIG. 6. Analysis of the high-frequency dielectric constant ε_∞ of wz-like Zn(O,S) alloys, determined from the Kramers-Kronig transformation of $\varepsilon_2(\omega)$. Solid line with asterisks shows the true $\varepsilon_\infty(x)$ of the alloy. The dashed line with filled circles describes the corresponding values for the unrelaxed alloys which show a more linear behavior; compare with Fig. 3. The dashed-dotted lines represent $\varepsilon_\infty(x)$ for hypothetic binaries of wz-ZnO (cross marks) and wz-ZnS (plus marks), where their $\varepsilon_2(\omega)$ spectra have been shifted on the energy scale to have the same band-gap energy $E_g(x)$ as the Zn(O,S) alloys. Moreover, the dotted line with diamonds is the linear combination of the two dashed-dotted lines.

one finds that $\varepsilon_\infty(x)$ is proportional to $1/E_g(x)$. Hence, the fact that the Zn(O,S) alloys do not exhibit stronger bowing of $\varepsilon_\infty(x)$ is a consequence of that the shape of $\varepsilon_2(\omega)$ changes significantly when the alloy composition x increases. The main contribution to the value of $\varepsilon_\infty(x)$, especially for large x, is the strong peak in $\varepsilon_2(\omega)$ at about 5–7 eV. To prove that, we analyze in detail the contribution from of $\varepsilon_2(\omega)$ to ε_∞ for wz-ZnO and wz-ZnS. ε_∞ is obtained by the Kramers-Kronig relations, which is given by 1 plus a term that involves the integration of $\varepsilon_2(\omega')$ over $0 \le \omega' < \infty$.[13] We split the integration into three integration regions, that is, the first region is from 0 to 4 eV, the second from 4 to 8 eV, and the third from 8 to 30 eV. We find that for wz-ZnO the three regions contribute to ε_∞ with about 0.0, 0.5, and 1.4 (i.e., 1%, 25%, and 74%), whereas for wz-ZnS the regions contribute with 0.0, 3.1, and 1.0 (i.e., 1%, 75%, and 24%), respectively. Thus, high energy region of the spectra contributes most for ZnO. For the S-rich (and also for Se-rich) compound, the strong ε_2 peak at 5–7 eV is important to the optical response as well as for the dielectric constant ε_∞ of the alloys.

The optical absorption coefficient is straightforwardly obtained from the dielectric function as $\alpha(\omega) = \sqrt{2}\omega c^{-1} \cdot [|\varepsilon(\omega)| - \varepsilon_1(\omega)]^{1/2}$. In Fig. 7, the calculated absorption spectra of wz-Zn(O,S) are presented for the low photon energy region and also for a broader energy region. The four other alloys have comparable spectra; see supplementary material[33] for corresponding figures. Since the absorption is related to the dielectric function, also the absorption spectra change in a well-behaved way with respect to sulfur content (i.e., compare with Fig. 5). In the energy region from 2 to 5 eV, the alloys show lower energy onset to absorption at the very band-gap energies. This is a consequence that the (O,S)-alloying does not form perfectly hybridized O-S like states at the VBM, and instead form

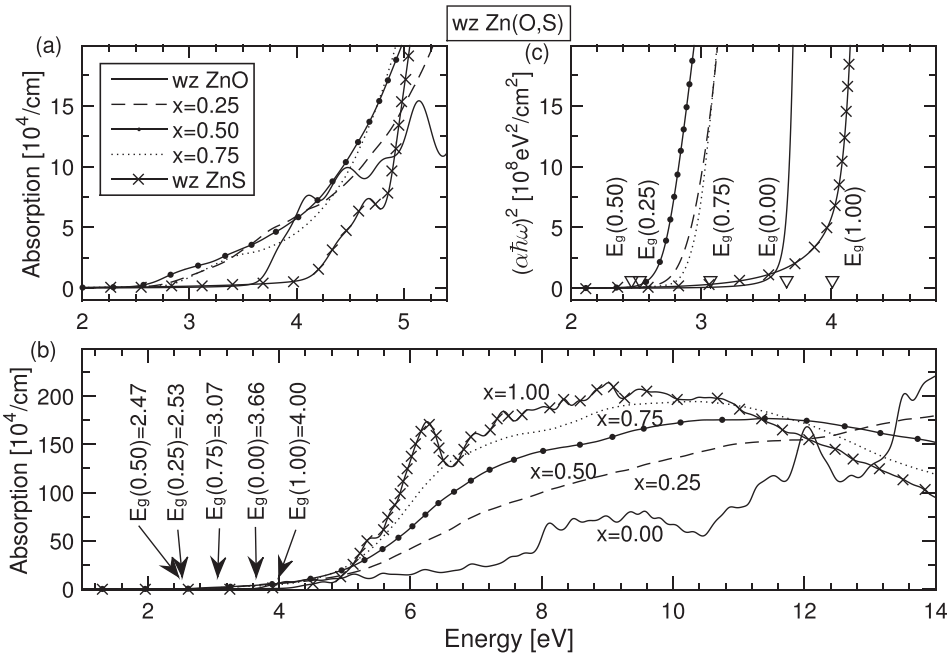

FIG. 7. The optical absorption coefficients $\alpha(\omega)$ of wz-like Zn(O,S) alloys obtained from the dielectric function in Fig. 5. In the upper-right figure, the $(\alpha(\omega)\cdot\hbar\omega)^2$ spectra demonstrate that the onset to absorption starts at the band-gap energy E_g in all the structures; the marks and arrows in the graph represent the values of E_g obtained from the Γ-point LDA+U energies. Zn(O,S) and Zn(O,Se) have qualitatively similar absorption coefficients, see supplementary material.[33]

partly ZnS-like semi-local states (cf. Fig. 4). The absorption of the alloy is somewhat weaker than the binary compounds near the gap energy, and that is a consequence of the semi-localized sulfur LDOS at the VBM (see Fig. 4). From the $(\alpha(\omega)\cdot\hbar\omega)^2$ spectra (upper-right graph), one notices that the energy onset to absorption follows the electronic band-gap energy, and this demonstrates that the alloys have direct band-gaps as verified also from the electron energy states. In the energy region 5 to 10 eV the change is monotonically increasing with respect to x, demonstrating a higher optical activity for the sulfur rich alloys for high photon energies. Overall, all alloy compounds show good optical absorption which indicates that the compounds form good band dispersion with no localized defect states. The absorption coefficient is relatively high near the band-gap energy for all the alloy compositions: $\alpha(\omega) > 5\times10^4\,\mathrm{cm}^{-1}$ for $\hbar\omega > E_g + 1.5\,\mathrm{eV}$. This demonstrates that Zn(O,Y) is suitable for optoelectronic applications, at the same time the band-gap value can be adjusted from almost 4 eV down to about 2.5 eV for Zn(O,S) and down to about 1.5 eV for Zn(O,Se). Since S- or Se-rich alloys have better absorption and the alloys have smaller gap energies, one can optimize the optoelectronic properties of the material.

Qualitatively, the calculated and available measured spectra[13] agree fairly well, however, with ZnO the main peak of $\varepsilon_2(\omega)$ at about 4−7 eV occurs about 0.5 eV lower in the experimental data (0.3 eV for ZnS and 0.7 eV for ZnSe). Of course, the applied LDA+U approach is expected not to exactly describe the positions of the energy peaks; however, we believe that this approach is sufficiently good in order to use it for large alloy systems. Here, we want to emphasize that we analyze the total energy of the alloys with regular LDA, and we use the LDA+U method (with correction on d- and s-orbital) in order to correct d-like states and also to artificially widen the gap. This is especially important for the Zn(O,Y) alloys, for which already moderated alloying content implies zero gap (and even "negative" gap) with the LDA. Modeling the alloys requires rather large supercells and hybrid functionals or GW approach for those supercells imply a too long computational time (and problem with computing memory), especially for optical properties that require large **k**-meshes and many empty bands. Here, it is also worth mentioning that even though GW and hybrid functionals approaches are more physically sounds, different GW approaches can generate different results, and especially the band-gap energy of ZnO has been found to be tricky to determine accurately. Also for hybrid functionals, like HSE06, the mixing and/or long-range screening parameter needs to be adjusted to describe ZnO properly.

The employed LDA+U method generates sufficiently accurate results qualitatively, however, in order to explore or justify that we compare the method with the scGW$_0$. In Fig. 8, we calculate the absorption spectra and the electronic band structures of the zb phase of ZnO, ZnS, and ZnSe binaries, using their unit cells and employ the scGW$_0$ approach as well from the LDA+U approach with two different settings of U: the first setting (denoted LDA+U$_d$+Δ_g) corrects properly only Zn d-like orbitals with U$_d$(Zn) = 6 eV and describes better the Zn-d – O-p hybridization.[37] Apart from that correction, LDA and LDA+U$_d$ give rather similar results. However, while regular LDA generates the gap energies $E_g = 0.74$, 2.14, and 1.30 eV for ZnO, ZnS, and ZnSe, respectively, the LDA+U$_d$ approach implies $E_g = 1.38$, 2.45, and 1.57 eV. With an additional "scissor operator" with constant energy shift $\Delta_g = 1.65$, 1.39, and 1.41 eV the gap energies are equal to the scGW$_0$ results of 3.03, 3.84, and 2.98 eV, respectively. The second setting (denoted LDA+U$_d$+U$_s$) corrects Zn d-like orbitals with U$_d$(Zn) = 10 eV, and an additional correction on the anion s-like orbitals with U$_s \approx -6$ eV to mimic the scGW$_0$ gap energies. The latter setting is used as the LDA+U approach is this work, and it gives a rough estimate of the band-gap energies.

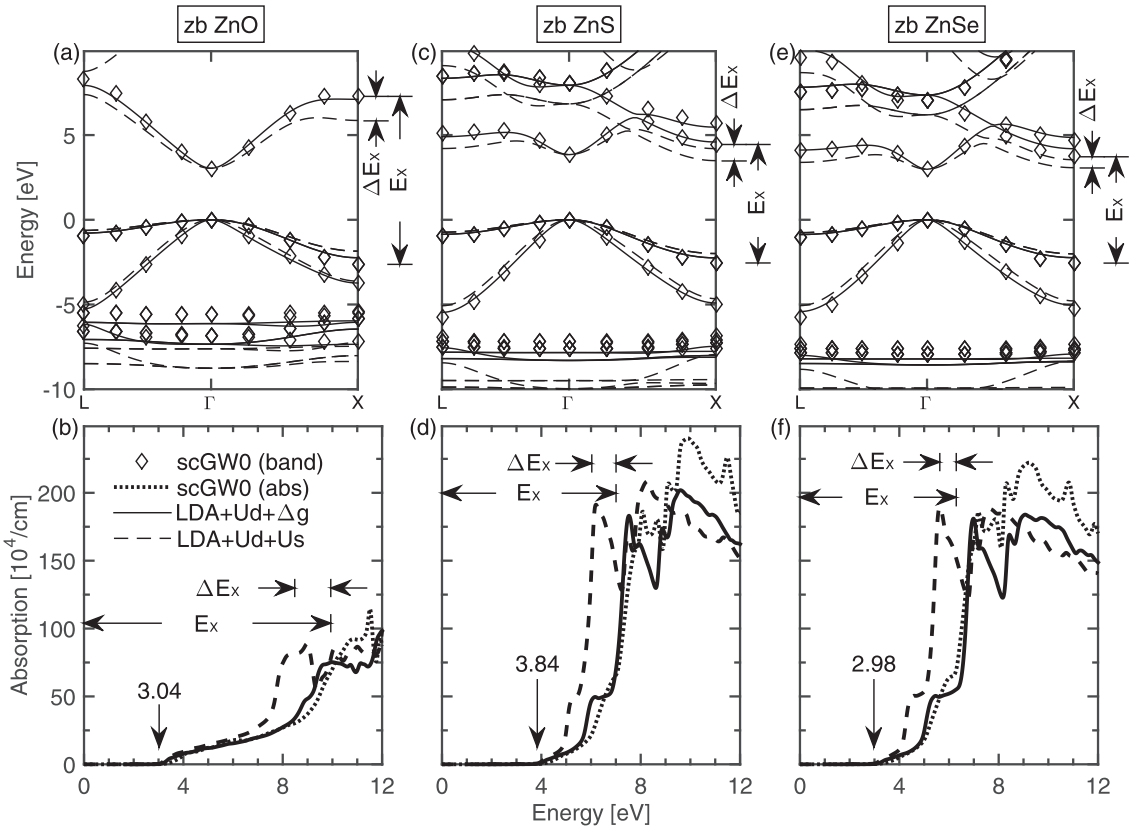

FIG. 8. Comparison of the electronic band structures as well as the absorption coefficients obtained from the $scGW_0$ approach (diamond marks and dotted lines) and two LDA+U approaches. The LDA+U_d+Δ_g (solid lines) fairly properly corrects the low-energy Zn *d*-like states at about −7 eV, but the gap has to be corrected by a constant shift Δ_g. LDA+U_d+U_s (dashed lines) generates better gap energies by applying a correction potential also for the anion *s*-like orbitals, but one observes that this approach yields lower energy position of the absorption peaks due to inaccurate band dispersions.

One observes in Fig. 8 that the LDA+U_d+Δ_g with the gap correction describes very well the band dispersion of both the CBs and the VBs. Therefore, also the absorption coefficients for LDA+U_d and $scGW_0$ agree rather well partly since the LDA+U_d+Δ_g absorption was shifted to the corresponding GW band-gap. Thereby, also regular LDA with proper gap correction will generate sufficiently good band structure and absorption spectra; however, LDA fails to accurately describe the energy levels of the Zn *d*-like states[37] and it will also underestimate the band curvature at the band edges (i.e., the effective electronic masses) due to too strong band coupling across the gap.[12] Also with the LDA+U_d+U_s method, the electronic band structures are comparable with that of $scGW_0$, but the Zn *d*-like states at −7 to −10 eV are energetically too low. That is mainly due to the strong U_d correction. More importantly, however, is that the band dispersion of the CBs away from the Γ-point deviates from the $scGW_0$ more than for LDA+U_d approach. For instance, at the X-point of the edge of the first Brillouin zone, the energy difference for the lowest CB between LDA+U_d+U_s and $scGW_0$ is $\Delta E_X \approx 1.4$, 1.0, and 0.7 eV for ZnO, ZnS, and ZnSe, respectively. The corresponding direct gap energy at the X-point is $E_X \approx 7.9$, 5.6, and 5.2 eV, obtained from the LDA+U_d+U_s potential, while the $scGW_0$ approach yields thus ΔE_X larger transition energies at that symmetry point. Since the optical transitions at the X-point contribute to the absorption peak at 5–8 eV, the LDA+U_d+U_s involves an inaccuracy due to the more flat energy dispersion of the lowest CB. This is considered in analyzing the dielectric function and the absorption coefficients of the Zn(O,*Y*) alloy. In some sense, this is a systematic error since we use the same approach for all systems. Moreover, the value of $\varepsilon_\infty(x)$ depends on the $\varepsilon_2(\omega)$ spectrum (which is directly related to $\alpha(\omega)$) and results from LDA+U_d+U_s and $scGW_0$ do not deviates too much. Also, the large energy shift of the band-gap is predicted by both the LDA+U_d+U_s and $scGW_0$ approaches.

IV. CONCLUSION

We have investigated the band-gap variation and the optical absorption of the $Zn(O,Y) \equiv ZnO_{1-x}Y_x$ alloys (Y = S and Se), by means of regular DFT and also of the partially self-consistent $scGW_0$ method. Both the hexagonal wz- and the cubic zb-like phases are considered, and these two phases have obviously very similar electronic and optical properties. The modeling of formation enthalpies indicates that the alloys can be synthesized, especially Zn(O,S) since the elemental sulfur atom is more comparable to the oxygen atom regarding atom size and electronegativity than the selenium atom.

Both sulfur and selenium incorporation in ZnO strongly widening the energy gap, and we demonstrate that the impact is due to local ionic relaxation to preserve the covalent bond lengths of the Zn–O and Zn–*Y* bonds. The calculated $scGW_0$ band-gap energies of the Zn(O,S) alloy agree very well with

available experimental results. The gap energy for the sulfur content $x = 0$, 0.5, and 1 are for wz-Zn(O,S) $E_g(x) \approx 3.1$, 2.4, and 3.9 eV, respectively, and corresponding experimental data is 3.4, 2.6, and 3.9 eV.[8,23] The zb-like alloy has somewhat smaller band-gap energies, $E_g(x) \approx 3.0$, 2.4, and 3.8 eV, respectively. For wz-Zn(O,Se), the scGW$_0$ gap energies for $x = 0$, 0.5, and 1 are $E_g(x) \approx 3.1$, 1.7, 3.0 eV, and for and zb-Zn(O,Se) the gap energies are 3.0, 1.0, and 3.0 eV. The present GW approach generates good gap energies; however, different types of GW approaches can imply deviation in the results. Nonetheless, we conclude that the band-gap of Zn(O,Se) can be narrowed to an energy that is suitable for solar energy technologies; for instance, the Shockley–Queisser limit indicates a maximum solar conversion efficiency for a single *pn*-junction with an absorbing material with a band-gap energy of 1.3–1.4 eV.

The strong band-gap narrowing in these alloys opens for a possibility to control the material optical properties with only moderate changes in the crystalline structure, basically only by lowering the crystalline symmetry by relaxation of the sp^3-hybridized bonds in the tetrahedral-like crystalline structure. For low or high alloying composition [i.e., in regions 1 and 3 in Fig. 4(d)], the change in the band-gap energy is described by the BAC model, while in the intermediate region (i.e., in region 2) the ABB model is a more proper description. This is an intuitively proper approach since the former model describes a local perturbation of the host compounds due to doping (or moderately alloying), while the latter model better describes the alloying with delocalized states; also the atomic-resolved LDOS supports the employed approach. From the fitting of the composition dependent band-gaps in Eq. (3), the boundary in wz-like Zn(O,S) between regions 1 and 2 is estimated to be $x_{12} \approx 0.06$ and the boundary between regions 2 and 3 is $x_{23} \approx 0.96$. zb-like Zn(O,S) has similar values: $x_{12} \approx 0.07$ and $x_{23} \approx 0.95$. Also, Se-based alloys present a similar effect with $x_{12} \approx 0.07$ and $x_{23} \approx 0.96$ for wz-like Zn(O,S), and $x_{12} \approx 0.06$ and $x_{23} \approx 0.97$ for zb-like Zn(O,Se). Thus, transitions between the different regions occur roughly at $x \approx 0.06$ and 0.96. This can define the regions for fully localized and fully delocalized region; however, there is an intermediate region where the alloying forms semi-local states.

The dielectric responses of the Zn(O,*Y*) demonstrate that the alloys have delocalized band dispersion without localized defect-like states, at least for a few percentage alloying composition. This generates relatively high absorption coefficients also in the lower energy region, which is suitable for optoelectronic properties. Despite the strong band-gap narrowing, the high-frequency dielectric constant ε_∞ increases fairly linearly as a function of sulfur content x. This is explained by the dielectric response in the alloys for energies above 5 eV, and the spectrum in this region determines to a large extent the value of ε_∞. Due to more flat energy dispersions of the lowest CBs in the S- and Se-rich alloys than in ZnO, the peak of the dielectric function around 5–6 eV is much larger for the S- and Se-rich alloys, thereby yielding larger ε_∞. The contribution to the static dielectric constant ε_0 depends on local ionic bonds and is less dependent of the response at higher energies. The dielectric constant for the sulfur content $x = 0$, 0.5, and 1 are for wz-Zn(O,S) $\varepsilon_0(x) \approx 7.6$, 8.7, and 7.4 and $\varepsilon_\infty(x) \approx 2.9$, 4.4, and 5.1, respectively. zb-Zn(O,S) has similar dielectric response: $\varepsilon_0(x) \approx 7.5$, 8.9, and 7.5 and $\varepsilon_\infty(x) \approx 3.0$, 4.5, and 5.1. Corresponding values for wz-Zn(O,Se) are $\varepsilon_0(x) \approx 7.6$, 10.0, and 8.6 and $\varepsilon_\infty(x) \approx 2.9$, 5.1, and 5.7 and values for zb-Zn(O,Se) are $\varepsilon_0(x) \approx 7.5$, 10.4, and 8.1 and $\varepsilon_\infty(x) \approx 3.0$, 5.2, and 5.8.

This work and earlier published studies on Zn(O,*Y*) with $Y = $ S or Se suggest that, despite that anion alloying of ZnO implies somewhat more distorted crystalline structure compared with cation alloying, the alloys are suitable for tuning the gap energy and optimizing or controlling material properties for various optoelectronic applications.

ACKNOWLEDGMENTS

We acknowledge the Swedish Energy Agency (Project No. 34138-1), the Swedish Research Council (Contract No. C0485101), and the Research Council of Norway (Project Nos. 239895 and 243642) for financial support, and the computer center NSC and USIT for high-performance computing resources via SNIC and NOTUR.

[1]V. Avrutin, D. J. Silversmith, and H. Morkoç, Proc. IEEE **98**, 1269 (2010).
[2]A. Janotti and C. G. Van de Walle, Phys. Rev. B **76**, 165202 (2007).
[3]Th. Gruber, C. Kirchner, R. Kling, F. Reuss, A. Waag, F. Bertram, D. Forster, J. Christen, and M. Schreck, Appl. Phys. Lett. **83**, 3290 (2003).
[4]A. Mohanta and R. K. Thareja, J. Appl. Phys. **103**, 024901 (2008).
[5]K. Ellmer, A. Klein, and B. Rech, *Transparent Conductive Zinc Oxide* (Springer, Berlin, 2008).
[6]C. Persson, C. Platzer-Björkman, J. Malmström, T. Törndahl, and M. Edoff, Phys. Rev. Lett. **97**, 146403 (2006).
[7]H. L. Pan, B. Yao, T. Yang, Y. Xu, B. Y. Zhang, W. W. Liu, and D. Z. Shen, Appl. Phys. Lett. **97**, 142101 (2010).
[8]O. Madelung, *Semiconductors: Data Handbook*, 3rd ed. (Springer, Berlin, 2004).
[9]P. E. Blöchl, Phys. Rev. B **50**, 17953 (1994).
[10]G. Kresse and D. Joubert, Phys. Rev. B **59**, 1758 (1999).
[11]M. Shishkin, M. Marsman, and G. Kresse, Phys. Rev. Lett. **99**, 246403 (2007).
[12]C. Persson and S. Mirbt, Br. J. Phys. **36**, 286 (2006).
[13]O. Madelung, U. Rössler, and M. Schulz, *Landolt-Börnstein III/41B Semiconductors II-VII, I-VII Compounds, Semimagnetic Compounds* (Springer, Berlin, 1999).
[14]M. B. Johansson, G. Baldissera, I. Valyukh, C. Persson, G. A. Niklasson, and L. Österlund, J. Phys.: Condens. Matter **25**, 205502 (2013).
[15]P. Pyykkö, Phys. Rev. B **85**, 024115 (2012).
[16]K. C. Mills, *Thermodynamic Data for Inorganic Sulphides, Selenides and Tellurides* (Butterworths, London, 1974), p. 60.
[17]S.-K. Kim, S.-Y. Jeong, and C.-R. Cho, Appl. Phys. Lett. **82**, 562 (2003).
[18]P. Villars and L. D. Calvert, *Pearson's Handbook of Crystallographic Data for Intermetallic Phases* (AMS, Metals Park, OH, 1985), Vol. 3, p. 3185.
[19]P. Atkins and J. de Paula, *Physical Chemistry*, 9th ed. (OUP, Oxford, 2010), p. 933.
[20]Y. He, L. Wang, L. Zhang, M. Li, X. Shang, Y. Fang, and C. Chen, J. Alloys Compd. **534**, 81 (2012).
[21]Y. He, L. Zhang, L. Wang, M. Li, X. Shang, X. Liu, Y. Lu, and B. K. Meyer, J. Alloys Compd. **587**, 369 (2014).
[22]S. K. Pandey, S. Pandey, V. Parashar, R. S. Yadav, G. K. Mehrota, and A. C. Pandey, Nanoscale **6**, 1602 (2014).
[23]B. K. Meyer, A. Polity, B. Farangis, Y. He, and D. Hasselkamp, Appl. Phys. Lett. **85**, 4929 (2004).
[24]R. R. Thankalekshmi and A. C. Rastogi, J. Appl. Phys. **112**, 063708 (2012).
[25]B. P. Burton, A. van de Walle, and U. Kattner, J. Appl. Phys. **100**, 113528 (2006).
[26]H. L. Pan, B. Yao, M. Ding, R. Deng, T. Yang, Y. R. Sui, T. T. Zhao, and L. L. Gao, J. Non-Cryst. Solids **356**, 906 (2010).

[27]M. Welna, R. Kudrawiec, Y. Nabetani, and W. Walukiewicz, Appl. Phys. Express **7**, 071202 (2014).
[28]W. Walukiewicz, W. Shan, K. M. Yu, J. W. Ager III, E. E. Haller, I. Miotkowski, M. J. Seong, H. Alawadhi, and A. K. Ramdas, Phys. Rev. Lett. **85**, 1552 (2000).
[29]W. Shan, W. Walukiewicz, J. W. Ager III, E. E. Haller, J. F. Geisz, D. J. Friedman, J. M. Olson, and S. R. Kurtz, Phys. Rev. Lett. **82**, 1221 (1999).
[30]X. F. Fan, Z. X. Shen, Y. M. Lu, and J.-L. Kuo, New J. Phys. **11**, 093008 (2009).
[31]C. Persson, R. Ahuja, and B. Johansson, Phys. Rev. B **64**, 033201 (2001).
[32]M. Dou, G. Baldissera, and C. Persson, Int. J. Hydrogen Energy **38**, 16727 (2013).
[33]See supplementary material at http://dx.doi.org/10.1063/1.4940700 for the dielectric function and the absorption spectra of the wz and zb phases of the Zn(O,S) and Zn(O,Se) alloys.
[34]F. Kootstra, P. L. de Boeji, and J. G. Snijders, Phys. Rev. B **62**, 7071 (2000).
[35]J. Serrano, A. H. Romero, F. J. Manjón, R. Lauck, M. Cardona, and A. Rubio, Phys. Rev. B **69**, 094306 (2004).
[36]M. Gajdos, K. Hummer, G. Kresse, J. Furthmuller, and F. Brechstedt, Phys. Rev. B **73**, 045112 (2006).
[37]C. Persson, C. L. Dong, L. Vayssieres, A. Augustsson, T. Schmitt, M. Mattesini, R. Ahuja, J. Nordgren, C. L. Chang, A. Ferreira da Silva, and J.-H. Guo, Microelectron. J. **37**, 686 (2006).